

Coastal cliff ground motions and response to extreme storm waves

Claire S. Earlie¹, Adam, P. Young², Gerd Masselink¹, Paul E. Russell¹

¹School of Marine Science and Engineering, Plymouth University, Plymouth, UK.

²Integrative Oceanography Division, Scripps Institution of Oceanography, University of California San Diego, La Jolla, California, USA.

Corresponding author: C. S. Earlie, School of Marine Sciences and Engineering, Plymouth University, Plymouth, England, PL4 8AA, UK. (claire.earlie@plymouth.ac.uk)

Key Points

- Coastal cliff ground motions are observed under extreme storm wave conditions ($H_s=6-8$ m)
- Under extreme wave conditions, vertical ground displacements can be in excess of 50 – 100 μm
- Erosion under extreme wave conditions is 2 orders of magnitude larger than the long-term erosion rate

Index Terms

3025 Marine Seismic, 0933 Remote Sensing, 1817 Extreme Events, 4546 Nearshore Processes

Keywords

Microseismic ground motion, Terrestrial Laser Scanning, extreme waves, cliff-top displacements, cliff-top wave overtopping, coastal erosion

An edited version of this paper was published by AGU. Copyright (2015) American Geophysical Union

Claire S. Earlie, Adam, P. Young, Gerd Masselink, Paul E. Russell, (2015) Coastal cliff ground motions and response to extreme storm waves, Geophysical Research Letters Digital Object Identifier 10.1002/2014GL062534 To view the published open abstract, go to <http://dx.doi.org> and enter the DOI.

Abstract

Coastal cliff erosion from storm waves is observed worldwide but the processes are notoriously difficult to measure during extreme storm wave conditions when most erosion normally occurs, limiting our understanding of cliff processes. Over January-February 2014, during the largest Atlantic storms in at least 60 years with deep water significant wave heights of 6 – 8 m, cliff-top ground motions showed vertical ground displacements in excess of 50 – 100 μm ; an order of magnitude larger than observations made previously. Repeat terrestrial laser scanner surveys over a 2-week period encompassing the extreme storms gave a cliff face volume loss 2 orders of magnitude larger than the long-term erosion rate. The results imply that erosion of coastal cliffs exposed to extreme storm waves is highly episodic and that long-term rates of cliff erosion will depend on the frequency and severity of extreme storm wave impacts.

1. Introduction and Background

Wave pressure fluctuations on the ocean floor generate microseismic ground motions both at the coast and hundreds of kilometers inland. Seismologists and oceanographers have used this ocean-driven microseismic activity as a proxy for hindcasting wave climate (Zopf *et al.*, 1976; Tillotson and Komar, 1997) since as far back as the 1930's (Gutenberg, 1931; Ramirez, 1940; Longuet-Higgins, 1950). More recently, combined observations of coastal ground motions and *in-situ* nearshore hydrodynamic data have advanced our understanding of ground motion on different coastal morphologies and shelf bathymetries under varying tidal and wave conditions (Adams *et al.*, 2002; Adams *et al.*, 2005; Young *et al.*, 2011; Dickson and Pentney, 2012; Young *et al.*, 2012; 2013; Norman *et al.*, 2013; Brain *et al.*, 2014). In most instances considered cliff-top ground motions increase with increasing wave height and tidal elevations.

The cliff-top ground motions generated from local ocean waves can be categorized into three major frequency bands: (1) high-frequency (HF) 1 – 50 Hz (1 – 0.02 s), reflecting the natural frequency of the ground as it ‘rings’ in direct response to wave impact and breaking waves (Young *et al.*, 2013); (2) low-frequency cliff motion or ‘‘flexing’’ generated by individual sea-swell or single-frequency waves (SF) 0.1 – 0.05 Hz (10 – 20 s) (Adams *et al.*, 2005); and (3) infragravity waves (IG) < 0.05 Hz (> 20 s) (Young *et al.*, 2011; 2012) which load the foreshore, causing pressure fluctuations. Microseisms are also detected and motions at double-frequencies (DF, twice the primary sea swell frequency) (0.1 – 0.2 Hz, 1 – 5 s) exhibit similar amplitude at the coast and tens of kilometers inland (Young *et al.*, 2011; Norman, 2012; Young *et al.*, 2013).

Cliff-top ground motions measured in wave conditions with significant wave height H_s less than 3 m show vertical ground displacements in the region of 0.5 – 10 μm during each wave

loading cycle (Adams *et al.*, 2005; Young *et al.*, 2011; Young *et al.*, 2013). It has been suggested that this repetitive flexure of the cliffs ultimately fatigues rock strength and leads to cliff failure (Adams *et al.*, 2005). Experiments using cross-shore seismometer arrays show an exponential decay in the ground motion signal (in the IG and SF bands) with distance inland (Adams *et al.*, 2005; Young *et al.*, 2011; Norman, 2012; Young *et al.*, 2012). The stresses created by the decrease of displacement inland are thought to be responsible for potentially weakening the integrity of the rock structure (Adams *et al.*, 2005). Brain *et al.* (2014) examined this hypothesis in sedimentary cliffs capped with glacial till deposits under a range of wave conditions ($H_s < 5$ m) and argued that ‘background’ microseismic cliff-top motion caused by cyclical loading is usually not of sufficient amplitude to drive growth of microcracks. However, Brain *et al.* (2014) also suggest larger displacements associated with episodic wave events ($H_s > 5$ m) can be responsible for less frequent, cliff-normal displacements, leading to an interaction between groups of microcracks that could ultimately damage the integrity of the rock structure.

Previous studies primarily focus on low to moderate incident ocean wave conditions and observations of the impacts of extreme wave events are rare. This study describes a unique set of observations made during exceptionally energetic storm conditions on a coastal cliff in the southwest U.K (occurring 31st Jan – 6th Feb 2014). The winter of 2014 was one of the most energetic periods the region has seen since the 1950’s (NOAA, 2014) and brought over 10 storms with significant wave heights in excess of 6 m (the 1% exceedance limit). This study relates cliff-top seismic observations to visual observations of storm wave activity using both *in-situ* and remote instrumentation. The cliff-top observations are placed in a longer-term context by comparing cliff-face changes that occurred over this extremely energetic period, obtained from terrestrial laser scanning, with the annual cliff-face development over the last 50 yrs.

1.1 Study Site

The study site (Fig. 1) is situated on the southwest peninsula of the UK along a 300-m stretch of uninhabited cliffed coastline southeast of Porthleven, UK. Facing southwest towards the Atlantic Ocean, the site is subject to a highly energetic wave climate, being exposed to both locally generated wind waves and Atlantic swell from the south and southwest (Scott *et al.*, 2011). The tidal regime is macrotidal with a mean spring range of 4.7 m. The cliffs are fronted by a steeply-sloping (slope 0.12) beach, formed of mainly flint of two classes: coarse to very coarse sand (1 – 2 mm) and fine to medium gravel (2 – 16 mm) (Buscombe and Scott, 2008). The cliffs rise 8 – 10 m above the beach, and the beach elevation at the cliff-toe varies from anywhere between 2 m and 4 m seasonally (in m Ordnance Datum Newlyn (ODN) which is *c.* 0.2 m above MSL).

The cliffs are mainly formed of Late Devonian Mylor slate lithofacies and comprise of pale grey-green mudstone with interbedded-siltstone and fine-grained sandstone (Leveridge and Shail, 2011) The cliffs are oriented at 200°, dipping gently southeastwards and exhibit evidence of deformation during the Variscan Orogeny (Alexander and Shail, 1996); cut by a variably reactivated network of late Carboniferous – Triassic fractures, joints and faults steeply dipping SSW and NNE (Fig. 1b). The Mylor slates are overlain by a *c.* 2 m thick Quaternary head deposit of poorly-consolidated clay, silt, sand and gravel capped with a thin layer of ‘made ground’ (0.3 – 0.5 m); a remnant of mining activity in the late 19th century (Cornwall County Council, 1999).

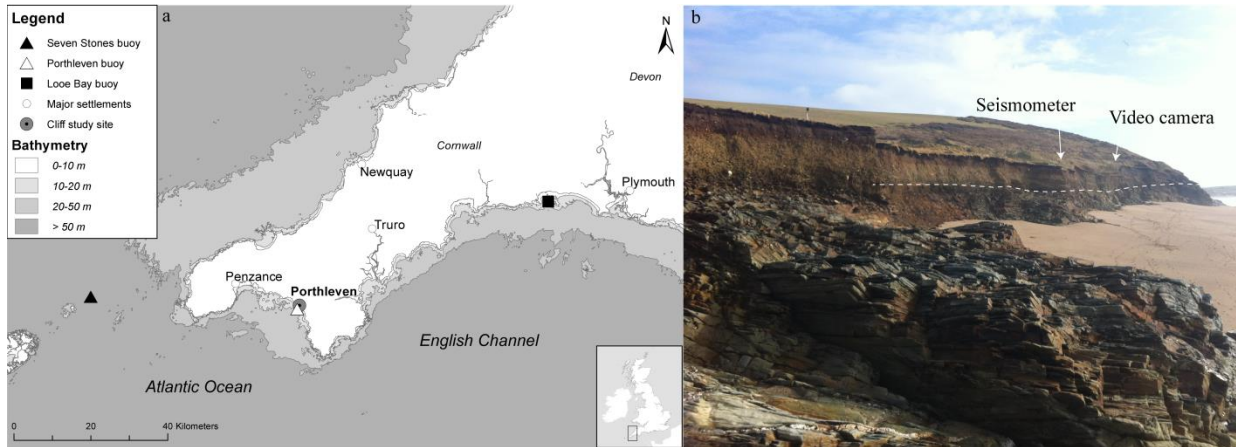


Figure 1 – (a) Study site with locations of nearshore and deep water wave buoys. (b) Photograph of site and locations of seismometer and video camera. The boundary between the two major geological units (Mylor slates and overlying Quaternary head deposits) is identified with a dotted line. Mylor Slate characteristics are shown in the outcrop in the foreground.

2. Methods

2.1 Wave climate

Deep water wave conditions were obtained from the Seven Stones offshore light-vessel located 55 km to the west of the site with a water depth of approximately 60 m (NOAA, 2014). Hourly statistics of offshore significant wave height were derived for the 7-day deployment duration. An inshore wave buoy located 1 km offshore (Porthleven buoy; Fig. 1a) worked for the first 5 days of the deployment, but malfunctioned following the exceptionally large waves on the night of 4th February. In order to extend the Porthleven wave record, the closest alternative inshore buoy situated 70 km ENE from the study site (Looe Bay directional wave buoy deployed in *c.* 10 m water depth; Fig 1a) was used. Over the available data period (2011 – 2014) significant wave heights at the Looe Bay buoy under southerly and southwesterly swell directions (180 – 225°) were only 5% smaller than the wave height measured at the Porthleven wave buoy. The inshore Looe Bay wave data were therefore considered representative for the wave conditions at Porthleven, and were deshoaled using linear wave theory to obtain deep water wave conditions. The deep water significant wave

height (H_s) and peak wave period (T_p) were subsequently used to compute the deep water wave energy flux (P) using (Komar, 1998; Masselink *et al.*, 2011):

$$P = \frac{1}{16} \rho g H_s^2 C_g \quad \text{Equation 1}$$

where ρ is the density of seawater (1025 kg/m³), g the gravitational acceleration (9.81 m/s²) and C_g the deep water group wave speed:

$$C_g = \frac{1}{2} \left(\frac{g T_p}{2\pi} \right) \quad \text{Equation 2}$$

2.2 Video capture

The slightly embayed nature of the cliffs provided a promontory from which a GoPro® waterproof video camera inside a closed-circuit television casing was deployed, facing north alongshore, towards the cliffs. The videos were GPS time-synced and closely inspected for cliff collapses, large wave impacts, and wave overtopping events for a 4:30 hour period as the tide dropped from high-tide to mid-tide during the most energetic storm wave event (5th Feb 2014). The video camera provided a qualitative, but detailed account of the hydrodynamics during the seismometer deployment.

2.3 Cliff-top ground motion

The cliff-top ground motion was recorded using a Nanometrics Compact Trillium broadband seismometer sampling at 100 Hz. The seismometer response has 3 dB corners at 0.0083 and 108 Hz. The instrument was buried in the Quaternary deposit in the cliff-top about 1 m below the ground surface, 5 m from the cliff-edge. The coastal cliff-top ground motions were compared with data obtained from the British Geological Survey inland broadband seismometer located at Carmellis, Cornwall 17 km inland from the site, sampling at 50 Hz (ORFEUS, 2014).

2.4 Seismic data processing

The raw ground vertical velocity data from the seismometer were corrected for phase and magnitude according to the instrument response curve. Hourly segments were band-passed in the frequency domain to investigate ground motions over three frequency bands: high-frequency (HF) 1 – 50 Hz, single-frequency (SF) 0.1 – 0.05 Hz, and infragravity-frequency (IG) 0.005 – 0.05 Hz. Double-frequency (DF) 0.1 – 0.2 Hz ground motions were also considered. The output velocity was integrated in the time domain to give ground displacement. Horizontal velocity data contains tilt effects at low-frequencies (Rogers, 1968; Webb and Crawford, 1999; Crawford and Webb, 2000) and have not been considered here.

2.5 Cliff-face volumes - Terrestrial laser scanning

Monthly scans of a 300-m cliff section at Porthleven were conducted using a Leica P20 terrestrial laser scanner over a 1-year period from July 2013 to July 2014 to enable linking the wave impacts on the cliff, to cliff development. Volumetric changes at the cliff-face were computed from these scans using a direct point-to-point cloud comparison method (Lague *et al.*, 2013).

3. Observations

3.1 Waves and water levels

The deep water wave buoy data presented in Figure 2a show two exceptionally large storm wave events within our 7-day window. At this buoy location, the first storm on 1st Feb had larger waves than the second storm on 5th Feb ($H_s > 10$ m, $T_p > 14$ s, compared to $H_s > 8$ m and $T_p > 12$ s, respectively); however, the wave direction during the second storm was more southerly, delivering more wave energy to the Porthleven coast. This is confirmed by the inshore wave buoy statistics, which show more energetic wave conditions during the second

storm ($H_s > 7$ m) compared to the first storm ($H_s > 5$ m). Maximum wave energy during both storms coincided with high-tide (Fig. 2a).

3.2 Cliff-top ground velocities and energy spectra

The cliff-top ground velocities increased with increasing incident wave height and tide level (Fig. 2b). The largest velocities occurred during the two extreme storm wave events on 1st and 5th Feb when significant wave heights offshore reached 6 – 8 m (Fig. 2a).

Comparison with inland seismic vertical velocity energy data (Fig. 2d) helped identify local and non-local sources of energy. Elevated HF signals were detected at the coast yet not inland, indicating a locally generated signal. The HF signals exhibited a tidal modulation and energy double peaks around 10 Hz and 20 Hz suggesting a possible primary normal site frequency of 10 Hz. Throughout the deployment, inland and coastal DF signals are similar suggesting a dominance of non-local signals at the coast, again, consistent with previous studies (i.e. Young *et al.*, 2013). At the coastal site, elevated SF ground motions (not detected inland) coincided with the storm events. The inland seismometer detected three peaks in the infragravity frequency range on the 1st, 2nd and 4th of February that were not detected at the coast, suggesting local inland source. The spectral peak located around 0.1 Hz on the 3rd Feb was present in both the inland and the coastal spectra and coincided with a magnitude 5.7 earthquake located at Lixourion, Greece (USGS, 2014). A clear IG energy peak occurred during the storm periods only in the coastal spectra (Fig. 2c).

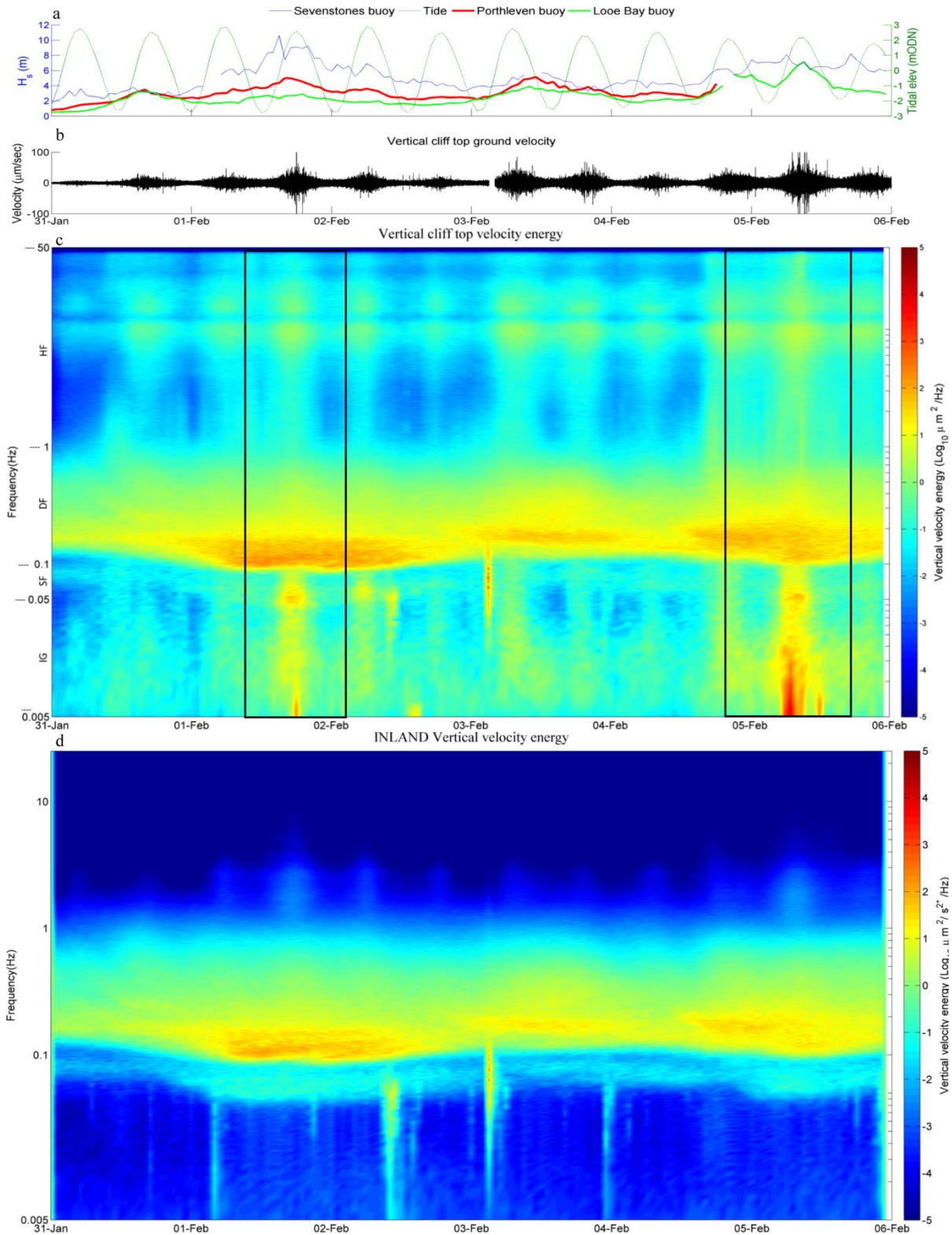


Figure 2 – (a) Tidal elevations (predicted) and significant wave heights from offshore wave buoy (blue) nearshore wave buoy at Looe Bay (green) and recorded (solid red line) Porthleven wave buoy. (b) Time series of vertical cliff-top ground velocity. (c) Spectra of vertical cliff-top velocity energy and (d) spectra of vertical velocity energy inland. The two rectangles on the spectra denote the most energetic storm wave periods.

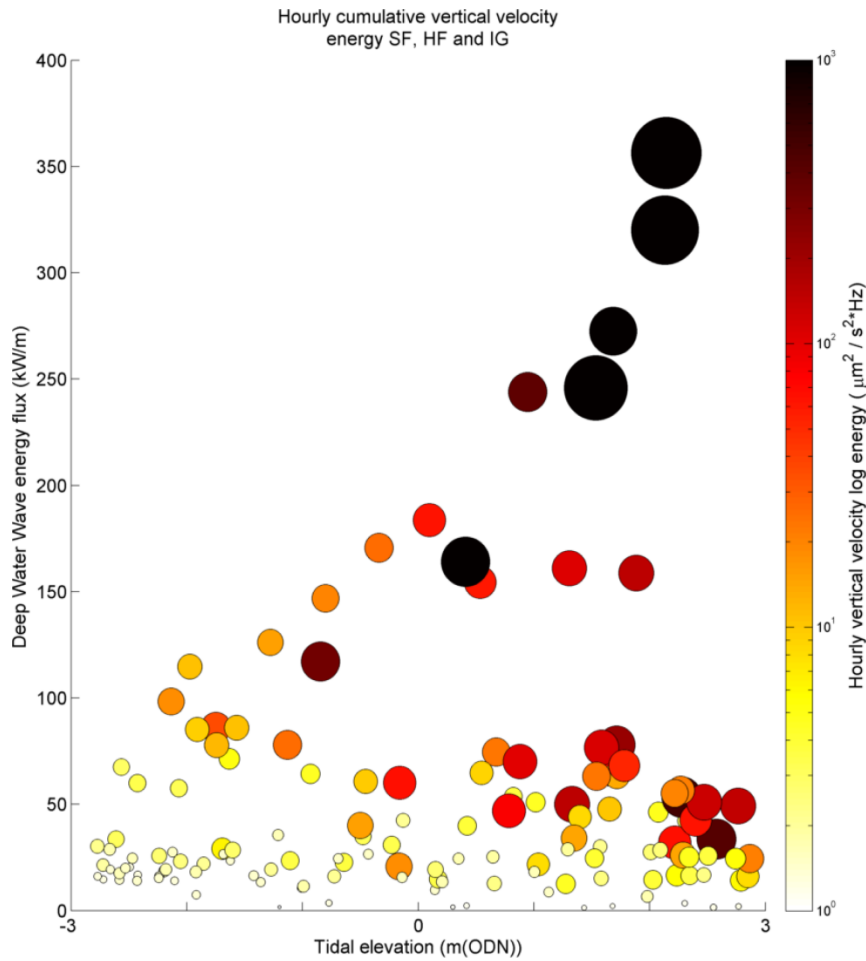


Figure 3 – Hourly total log vertical velocity energy (between 50 and 0.005 Hz) excluding double frequencies (0.2 – 0.1 Hz) at various states of tide and deep water wave energy flux (calculated using Eqns. 1 and 2). Vertical velocity energy is scaled by color and size of the bubble, and plotted logarithmically as the energy increases by orders of magnitude during the extreme events.

The total hourly vertical velocity energy is a function of both incident wave energy and the tidal elevation (Fig. 3). Lower-energy values are seen at all states of tide, yet only associated with lower wave energy flux (< 100 kW/m). The highest velocity energy (an order of magnitude greater than ‘normal’) only occurs during very energetic wave conditions and during higher tidal elevations (where cliff-top velocity energy exceeded $1000 \mu\text{m}^2/\text{s}^2/\text{Hz}$ and wave power exceeded 200 kW/m). The largest contribution during energetic wave conditions and at higher tidal elevations is from energy at infragravity-frequencies.

3.3 Displacements under extreme wave conditions

In previous cliff-top ground motion studies with significant wave heights up to 5 m, vertical displacements rarely exceeded 10 μm (Adams *et al.*, 2005; Young *et al.*, 2011; Young *et al.*, 2013). At our site, ground displacements during both the extreme storm wave events increased by an order of magnitude (Fig. 4b), where the vertical displacements increased from 5 – 10 μm under calmer periods to > 50 μm under energetic conditions. These greatest vertical displacements occurred during the second storm event at high-tide (Fig. 2 and Fig 4. from 08:00 on the 5th Feb 2014).

The camera footage captured during the 5th February storm event shows different wave conditions including: (1) wave breaking on the beach; (2) wave breaking at the cliff-toe; and (3) overtopping of the entire cliff elevation. Timings of visible cliff collapses were also recorded (Fig 4a and movie clip provided as supplementary material).

Under energetic conditions the largest vertical displacements (Fig. 4b) were coincident with periods of successive cliff overtopping followed by water cascading down the cliff-face. This suggests wave loading and unloading on the cliff-top might significantly increase cliff motion and the associated strains and flexure mechanisms during times of wave overtopping at higher tidal elevations.

Peaks in IG and HF signals also coincided with time periods of successive overtopping and subsequent cascading events (Fig. 4c and e at 08:15 and 09:05 hrs.). However, not all overtopping events caused significantly elevated signals. Elevated SF signals occurred during some time periods of wave overtopping, but the signal variation was less clear compared to timings of the peaks in the IG and HF signals.

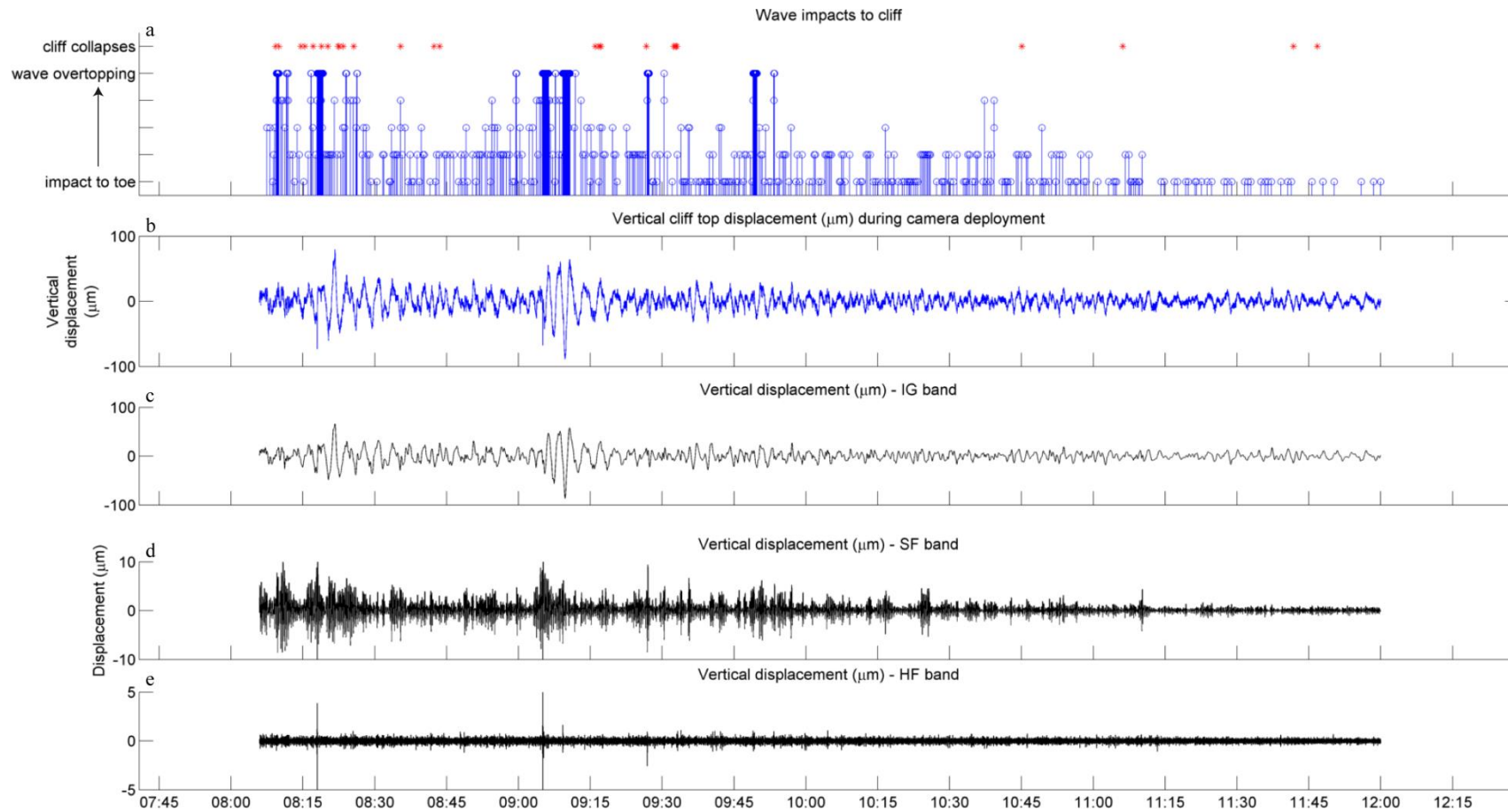


Figure 4 – (a) Wave impacts to the cliff characterized using the video camera footage, y-axis represents a gradual increase in height of wave impact up cliff face, from impact to the toe to overtopping cliff-top, red dots indicate timings of cliff failures. Time series of vertical cliff-top displacement during camera deployment period (08:00 to 12:30 hrs. on 5th February 2014): (b) across all frequency bands (0.005 – 50Hz), (c) infragravity band IG (0.005 – 0.5 Hz), (d) single-frequency band SF (0.1 – 0.05 Hz) and (e) high-frequency band HF (1 – 50 Hz). High-tide on the 5th Feb occurred at 8.31am.

1 During each overtopping event, the camera footage showed large volumes of water impacting
2 the top of the cliff and cascading down the cliff-face for a limited amount of time (from
3 anywhere between 10 seconds to 2 minutes), the duration of which depended on the scale of
4 overtopping (Fig. 5a). The camera footage commenced 30 mins prior to the peak of the high-
5 tide. Wave overtopping was recorded from this point and for up to 90 mins after the peak of
6 the tide. Although cliff collapses cannot be directly coupled with ground displacements, there
7 appeared to be a period of time around the high-tide where the majority of failures and wave
8 overtopping occurred. Ground displacement increased in magnitude over this period of
9 elevated tidal levels, suggesting that the cliff underwent an amplified series of strains and
10 flexure mechanisms during times of wave overtopping. Although the timings of the intensive
11 ground placements did not coincide exactly with the cliff failures, the period of energetic cliff
12 motion coincided with the period of frequent cliff failures.

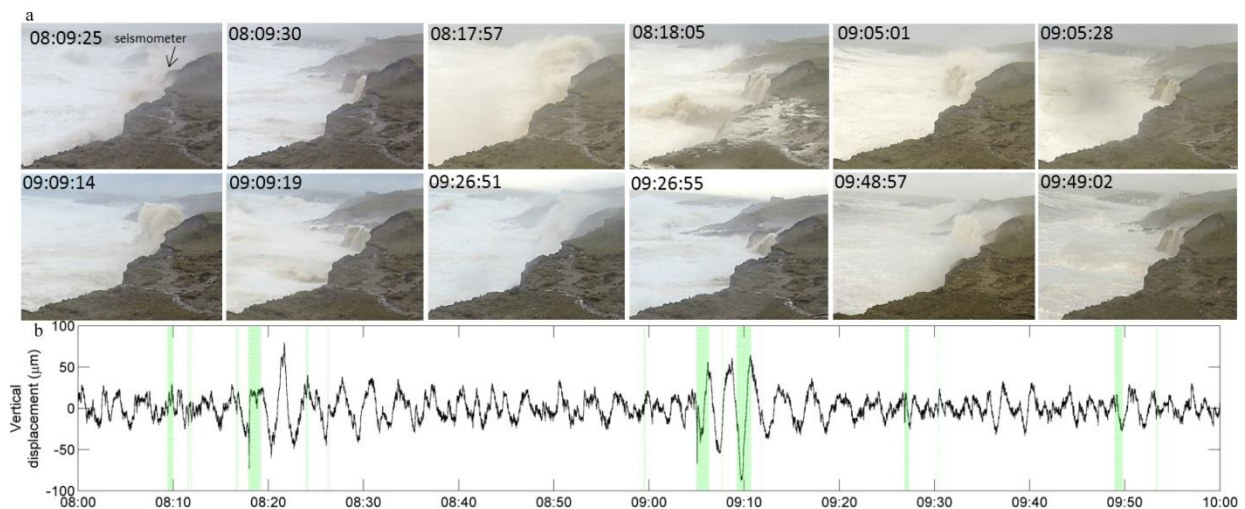


Figure 5 - (a) Stills from camera footage, illustrating successive wave overtopping and subsequent drainage events on the 5th February 2014 from 08:09 to 09:49 hrs. Overtopped water cascading down the cliff-face seen in the stills corresponds with the shaded regions of plot b. (b) Vertical displacement during this period. A 60-sec movie clip during the camera deployment is provided as supplementary material.

13 **4. Geomorphic perspective and relation to cliff-face development**

14 The consequences of these unusually large-scale cliff-top displacements (50 – 100 µm) under
15 the largest wave conditions seen in 60 yrs in terms of rock damage from coastal flexing are

16 unknown. However, previous research has suggested that although displacements under
17 'normal' conditions are not likely to contribute towards weakening of rock structures,
18 episodic displacements caused by extreme wave conditions may be responsible for failure in
19 metasedimentary cliffs (Brain *et al.*, 2014).

20 The long-term annual retreat rate for Porthleven, obtained from aerial photography and
21 averaged over 50 yrs (Ridgewell and Walkden, 2009), is 0.1 myr^{-1} . This value was
22 corroborated by Earlie *et al.* (2014) using airborne LiDAR over a 3.5 year period (0.09 myr^{-1}).
23 Assuming a cliff height of 10 m, a long-term cliff recession rate of 0.1 m yr^{-1} equates to an
24 annual cliff volumetric loss of 1 m^3 per m length of cliff. Terrestrial laser scans over the 2-
25 week storm period show that the 300-m long cliff section eroded 1350 m^3 , which represents
26 4.5 m^3 average erosion volume per m length of cliff over the 2-week period, or an annual cliff
27 volumetric loss of 113 m^3 per m length of cliff. The annual cliff volumetric loss over the 2-
28 week storm period is therefore two orders of magnitude greater than volumetric loss based on
29 the long-term cliff recession (i.e., $113 \text{ m}^3 \text{ m}^{-1} \text{ yr}^{-1}$ versus $1 \text{ m}^3 \text{ m}^{-1} \text{ yr}^{-1}$).

30 During the 4.5-hour camera deployment the video footage clearly shows failure of cliff
31 material throughout with over 30 failures recorded when energetic wave conditions and
32 regular cliff overtopping prevailed; such cliff failure is not observed under calmer conditions,
33 even at high-tide. This strongly suggests that the observed cliff failures have been triggered
34 by the direct combination of wave impacts and overtopping, and possibly facilitated by the
35 weakening of the cliff through microcrack density growth, such as suggested by Adams *et al.*
36 (2005) and Brain *et al.* (2014). The significance of these extreme wave events on erosion cliff
37 morphology is further highlighted by the observation that the total erosion volume over the 2-
38 week storm period not only exceeds the long-term erosion rate by two orders of magnitude
39 but also accounts for more than half (53%) of the total volumetric loss for the year 2013 –
40 2014 with reportedly the most severe winter wave conditions on record.

41 **5. Conclusions**

42 Vertical cliff-top ground motions measured during an exceptionally stormy winter period in
43 the UK were found to increase with increasing H_s and tidal elevation. During extreme wave
44 conditions (H_s exceeding 6 m) vertical ground displacements increased by an order of
45 magnitude from 10 μm to 100 μm . Real time cliff-top video capture allowed for association
46 of these large ground displacements with the nearshore hydrodynamics and in particular cliff-
47 top wave overtopping events. The greatest ground motion contribution ($\sim 100 \mu\text{m}$) originated
48 from displacements in the infragravity-frequencies (0.5 – 0.005 Hz). The displacement peaks
49 in the single-frequencies (0.1 – 0.05 Hz) of 10 μm and high-frequencies (1 – 50 Hz) of 5 μm
50 also coincided with the timings of the wave overtopping events captured with the video
51 camera. Cliff-face volume erosion measured over a 2-week storm period, encompassing the
52 two extreme events discussed in this study, exceeded the long-term erosion rate by two orders
53 of magnitude, providing a geomorphic link between energetic cliff-top ground displacements
54 and cliff failure.

55 Capturing these events during one of the stormiest periods the region has seen in 60 years,
56 highlights the role extreme events play in contributing towards coastal cliff erosion. Having
57 recorded microseismic cliff-top motion on this scale for the first time and determined an
58 effective method of monitoring the energetic wave impacts *in-situ*, emphasizes how further
59 investigation of cliff behavior during storms is not only obtainable, but paramount to
60 understanding coastal evolution under extreme conditions.

61 **Acknowledgements**

62 This work was funded by Plymouth University School of Marine Science and Engineering
63 small research grant; *Storm wave impacts on coastal cliffs*. Wave data are available from the
64 Channel Coastal Observatory, inland seismic data from British Geological Survey and coastal

65 seismic data are available upon request from the authors. We gratefully thank Pedro Almeida,
66 Tim Poate, Kit Stokes, Peter Ganderton, Robin Shail and Mike Hardy for invaluable field
67 assistance under adventurous conditions.

68 **References**

- 69 Adams, P.N., Anderson, R.S., and Revenaugh, J., (2002), Microseismic measurement of
70 wave-energy delivery to a rocky coast, *Geology*, **30**, pp. 895 – 898
- 71 Adams, P.N., Storlazzi, C.D., and Anderson, R.S., (2005) Nearshore wave induced cyclical
72 flexing of sea cliffs, *Journal of Geophysical Research*, **110**
- 73 Brain, M.J., Rosser, N.J., Norman, E.C., and Petley, D.N., (2014), Are microseismic ground
74 displacements a significant geomorphic agent? *Geomorphology*, **207**, pp. 161 – 173.
- 75 Buscombe, D.D., and Scott, T.M., (2008), *The Coastal Geomorphology of North Cornwall:
76 St. Ives Head to Trevoze Head*, Wave Hub Impact on Seabed and Shoreline Processes
77 (WHISSP), University of Plymouth.
- 78 Cornwall County Council, (1999), *Cornwall Industrial Settlements Initiative: Porthleven*,
79 Historic Environment Service, Cornwall County Council.
- 80 Crawford, W.C., and Webb, S.C., (2000) Identifying and removing tilt noise from low-
81 frequency (<0.1 Hz) seafloor vertical seismic data, *Bull., Seismol., Soc., Am.*, **90**(4), pp. 952 –
82 963.
- 83 Dickson, M.E., and Pentney, R., (2012) Micro-seismic measurements of cliff motion under
84 wave impact and implications for the development of near-horizontal shore platforms,
85 *Geology*, **151- 152**, pp. 27 – 38.
- 86 Earlie, C.S., Masselink, G., Russell, P.E., Shail, R.K., (2014) Application of airborne LiDAR
87 to investigate rates of recession in rocky coast environments, *Journal of Coastal
88 Conservation*, DOI 10.1007/s11852-014-0340-1
- 89 Gutenberg, B., (1931), *Bulletin of the Seismological Society of America*, **21**, 1.
- 90 Komar, P.D., (1998). *Beach Processes and Sedimentation*, 2nd edn. Upper Saddle River, NJ:
91 Prentice-Hall.
- 92 Lague D., Brodu, N., Leroux., J, (2013), Accurate 3D comparison of complex topography
93 with terrestrial laser scanner : application to the Rangitikei canyon (NZ), *ISPRS Journal of
94 Photogrammetry and Remote Sensing*, **80**, pp. 10 – 26.
- 95 Leveridge, B.E., Shail R.K., (2011), The Gramscatho Basin, south Cornwall, UK: Devonian
96 active margin successions, *Proceedings of the Geologists' Association*, **122**, pp. 568–615.
- 97 Longuet-Higgins, M.S., (1950), A theory of the origin of microseisms, *Phil. Trans. R. Soc.*
98 **243**, 1–35.

- 99 Masselink, G., Hughes, M.G., and Knight J., 2011. *Introduction to Coastal Processes and*
100 *Geomorphology* 2nd ed. Hodder Education, London.
- 101 NOAA, (2014), National Oceanographic and Atmospheric Administration, National Data
102 Buoy Centre, Station 62107 – Sevenstones Lightship,
103 <http://www.ndbc.noaa.gov/station_page.php?station=62107> [March 2014]
- 104 Norman, E.C., (2012) Microseismic monitoring of the controls on coastal rock cliff erosion,
105 PhD Thesis, Department of Geography, Durham University.
- 106 ORFEUS, (2014), Observatories and research facilities for European Seismology, European
107 Integrated Data Archive, Available from: <<http://145.23.252.222/eida/webdc3/>>[June 2014].
- 108 Ramirez, J. E., (1940), An experimental investigation of the nature and origin of microseisms
109 at St. Louis, Missouri. *Bulletin of the Seismological Society of America*. **30**, 35 – 84, 139 –
110 178.
- 111 Rodgers, P. W. (1968), Response of horizontal pendulum seismometer to rayleigh and love
112 waves tilt and free oscillations of Earth, *Bulletin of the Seismological Society of America*,
113 **58**(5), 1384 – 1406.
- 114 Scott, T., Masselink, G., Russell, P., (2011), Morphodynamic characteristics and
115 classification of beaches in England and Wales, *Marine Geology*, **286**, pp. 1 – 20.
- 116 Tillotson, K., and Komar, P.D., (1997), The wave climate of the Pacific Northwest (Oregon
117 and Washington): A comparison of data sources: *Journal of Coastal Research*, **13**, pp. 440–
118 452.
- 119 USGS, (2014), Earthquake Hazards Program, Available from:
120 <<http://comcat.cr.usgs.gov/earthquakes/eventpage/usc000mfuh#pager>> [October 2014].
- 121 Webb, S.C., and Crawford, W.C., (1999), Long-period seafloor seismology and deformation
122 under ocean waves, *Bull. Seismol. Soc. Am.*, **89**(6), pp. 1535 – 1542.
- 123 Young, A.P., Adams, P.N., O'Reilly, W.C., Flick, R.E., and Guza, R.T., (2011) Coastal cliff
124 ground motions from local ocean swell and infragravity waves in southern California,
125 *Journal of Geophysical Research*, **116**.
- 126 Young, A.P., Guza, R.T., Adams, P.A., O'Reilly, W.C., Flick, R.E., (2012), Cross-shore
127 decay of cliff top ground motions driven by local ocean swell and infragravity waves,
128 *Journal of Geophysical Research*, **117**
- 129 Young, A.P., Guza, R.T., Dickson, M.E., O'Reilly, W.C., and Flick, R.E., (2013) Ground
130 motions on rocky, cliffed, and sandy shorelines generated by ocean waves, *Journal of*
131 *Geophysical Research: Oceans*, **118**, pp. 6590 – 6620.
- 132 Zopf, D.O., Creech, H.C., and Quinn, W.H., (1976), The wavemeter: A land-based system for
133 measuring nearshore ocean waves: *Marine Technological Society Journal*, **10**, pp. 19–25.
- 134
- 135

136 **Figure Captions**

137 Figure 1 – (a) Study site with locations of nearshore and deep water wave buoys. (b)
138 Photograph of site and locations of seismometer and video camera. The boundary between
139 the two major geological units (Mylor slates and overlying Quaternary head deposits) is
140 identified with a dotted line. Mylor Slate characteristics are shown in the outcrop in the
141 foreground.

142 Figure 2 – (a) Tidal elevations (predicted) and significant wave heights from offshore wave
143 buoy (blue) nearshore wave buoy at Looe Bay (green) and recorded (solid red line)
144 Porthleven wave buoy. (b) Time series of vertical cliff-top ground velocity. (c) Spectra of
145 vertical cliff-top velocity energy and (d) spectra of vertical velocity energy inland. The two
146 rectangles on the spectra denote the most energetic storm wave periods.

147 Figure 3 – Hourly total log vertical velocity energy (between 50 and 0.005 Hz) excluding
148 double-frequencies (0.2 – 0.1 Hz) at various states of tide and deep water wave energy flux
149 (calculated using Eqns. 1-2). Vertical velocity energy is scaled by color and size of the
150 bubble, and plotted logarithmically as the energy increases by orders of magnitude during the
151 extreme events.

152 Figure 4 – (a) Wave impacts to the cliff characterized using the video camera footage, y-axis
153 represents a gradual increase in height of wave impact up the cliff face, from impact to the
154 toe to overtopping cliff-top, red dots indicate timings of cliff failures. Time series of vertical
155 cliff-top displacement during camera deployment period (08:00 to 12:30 hrs. on 5th February
156 2014): (b) across all frequency bands (0.005 – 50Hz), (c) infragravity band IG (0.005 – 0.5
157 Hz), (d) single-frequency band SF (0.1 – 0.05 Hz) and (e) high-frequency band HF (1 – 50
158 Hz). High-tide on the 5th Feb occurred at 8.31am.

159 Figure 5 - (a) Stills from camera footage, illustrating successive wave overtopping and
160 subsequent drainage events on the 5th February 2014 from 08:09 to 09:49 hrs. Overtopped
161 water cascading down the cliff-face corresponds with the shaded regions of plot b. (b)
162 Vertical displacement during this period. A 60-sec. movie clip during the camera deployment
163 is provided as supplementary material.